Atomic-scale mechanisms of plasma-assisted elimination of nascent base-grown carbon nanotubes

Atomic-scale mechanisms of plasma-assisted elimination of nascent base-grown carbon nanotubes

Umedjon Khalilov*, Annemie Bogaerts and Erik C. Neyts*

Research Group PLASMANT, Department of Chemistry, University of Antwerp,

Universiteitsplein 1, 2610 Wilrijk, Antwerp, Belgium

Abstract

Selective etching allows for obtaining carbon nanotubes with a specific chirality. While plasma-assisted etching has already been used to separate metallic tubes from their semiconducting counterparts, little is known about the nanoscale mechanisms of the etching process. We combine (reactive) molecular dynamics (MD) and force-bias Monte Carlo (tfMC) simulations to study H-etching of CNTs. In particular, during the hydrogenation and subsequent etching of both the carbon cap and the tube, they sequentially transform to different carbon nanostructures, including carbon nanosheet, nanowall, and polyyne chains, before they are completely removed from the surface of a substrate-bound Ni-nanocluster. We also found that onset of the etching process is different in the cases of the cap and the tube, although the overall etching scenario is similar in both cases. The entire hydrogenation/etching process for both cases is analysed in detail, comparing with available theoretical and experimental evidences.

*Corresponding authors. E-mail: umedjon.khalilov@uantwerpen.be (Umedjon Khalilov);

E-mail: erik.neyts@uantwerpen.be (Erik C. Neyts)

1. Introduction

Due to their chirality-dependent properties, many applications of carbon nanotubes (CNTs) require to control their synthesis at the nanoscale level. While a precise control over the resulting structure is still a daunting task, current synthesis techniques, including arc discharge, laser ablation, fullerene recrystallization and chemical vapour deposition (CVD), are producing nanotubes with well-defined structures to a certain extent [1-4]. Due to its simplicity, high degree of control and scalability, the CVD method currently is the most common experimental technique to growth CNTs [5, 6]. In general, CVD can be divided into two types: thermal CVD, in which a hydrocarbon gas is catalytically dissociated at the nanocatalyst surface at elevated temperature [7-9] and plasma CVD, in which the source gas decomposition is effectively carried out in the plasma phase by ion, radical and electron impacts without the need for additional thermal energy [10-13]. Although plasma CVD offers some advantages over thermal CVD, such as possible control over the alignment of the CNTs in free-standing form due to the strong electric fields [11, 14-16] or growth at reduced temperature [17-19], the obtained carbon structures are easily eliminated as well due to the high fluxes of radicals or ions [20, 21]. Hence, under plasma conditions, the net growth kinetics of CNTs can be expressed as a balance between the growth and etching processes [21].

In particular, the role of hydrogen is significant in plasma-assisted CNT growth, since it can amorphize or hinder the formation of graphite-like carbon, if its concentration is too high [22]. Specifically, H atoms cause the breaking of the sp^2 C-C bonds and the formation of sp^3 C-H bonds, resulting in CNT etching [23]. Behr and colleagues reported that incident H atoms from a H_2 plasma preferentially amorphize and etch both graphite and CNT [24]. The authors indicated that once an etch pit is formed, the etching proceeds rapidly, and the remainder of the CNT is

quickly etched away. On the other hand, plasma etching can also be utilized either to eliminate unwanted small nanotubes or to separate semiconducting tubes from their metallic counterpart. Zhang and co-workers for instance reported the selective etching of metallic nanotubes, retaining the semiconducting nanotubes in near-pristine form using neutral and positive ions of H and CH_3 species in methane plasma [23]. Also, Hou and co-workers obtained small-diameter semiconducting and large-diameter metallic tubes by tuning experimental parameters using hydrogen as an etchant gas [25].

It is therefore clear that structural control of CNTs is complex, due to the role of hydrogen in plasma CVD: the etching simultaneously occurs during CNT growth [21, 26]. Also, *in-situ* transmission electron microscopy (TEM) observations showed that in particular the cap formation is critical in the growth and structural control of single-wall CNT (SWNT) using H-containing carbon precursors [27-29]. However, the incubation period of the nucleation stage can be prolonged, or "incipient" carbon-based structures can even be completely removed from the catalyst surface, in both thermal and plasma CVD growth by the presence of hydrogen [21, 27, 29, 30]. Nevertheless, the precise etching mechanism in the early stages of CNT growth and its etching nature is still not fully understood, which is very important to understand the CNT nucleation process in a plasma setup [31, 32]. We here address the etching mechanisms of different carbon nanostructures at different growth stages of SWNTs, specifically comparing the etching behaviours of carbon caps, small and long nanotubes.

2. Computational details

The hydrogenation and etching processes are investigated by combined (reactive) molecular dynamics (MD) and force-bias Monte Carlo (tfMC) [33, 34] simulations. The temperature is controlled at 1600 K by the canonical Bussi thermostat [35]. In the simulations, all atomic interactions are described by the ReaxFF force field, using parameters developed by Mueller et al. [36], and which have previously been demonstrated to be suitable for this system [29, 37, 38].

Prior to hydrogenation, a carbon cap of a (5,5) or (10,0) tube, as well as different grown cap structures on either a small (Ni_{55}) or a large (Ni_{147}) nanoparticle, are physisorbed on a virtual Al substrate [38]. Also, (5,5) and (10,0) tubes are positioned on the substrate-bound catalyst cluster (see Supplementary Figure 1), thereby mimicking catalysed base growth experiments. Also, we use two "tube/cluster" modes: a tangential mode, where the tube diameter is close to that of the cluster, and a perpendicular one with the tube smaller than the cluster diameter, which correspond to experimental observations [39]. In all cases, the cluster diameter is about 1.2-1.6 times larger than the diameter of the carbon structure, which is in an excellent agreement with both experimental and theoretical observations [40, 41].

Since the concentration of H-atoms is significant in a hydrogen plasma [42], and since H-atoms are much more reactive than H_2 molecules, we here solely use H-atoms as gas-phase species surrounding the catalyst and tube in order to understand the individual effect of H-radicals. In the MD simulations, the concentration of H-atoms is kept constant at any moment. When an H-atom adsorbs on the nanotube or the cluster particle, the resulting structure is allowed to relax by application of tfMC. During this relaxation stage, no new H atoms are allowed to impinge on the tube. Also, gas phase etching products are removed every 10^6 MD steps to prevent pyrolysis reactions.

3. Results and discussion

3.1 Elimination of a carbon cap. Figure 1 shows the overall hydrogenation/etching process of a carbon cap. The hydrogenation/etching process can be divided in four stages, in which different carbon/nickel structures can be distinguished. Initially, a (5,5) carbon cap (C_{40}) on a carbon-containing nickel ($Ni_{55}C_{19}$) cluster is hydrogenated (stage I) and gradually transforms into a carbon nanosheet (stage II). Subsequently, the carbon nanosheet can transform to free-standing graphene patch(es) or a carbon nanowall. Finally, only simple carbon structures, including vertically-aligned carbon rings or carbon polyyne chains, as well as pentagon/hexagon rings, remain (stage III), prior the total removal of any carbon structures from the catalyst surface (stage IV).

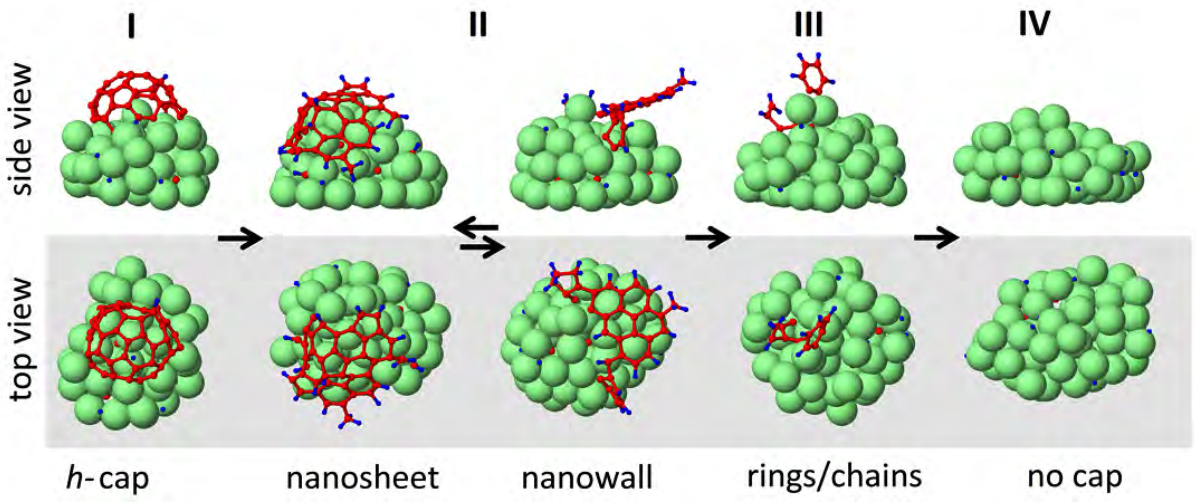

Figure 1 Sequential transformation of a carbon cap into nanosheet, nanowall and initial carbon structures prior to cap elimination from the catalyst surface in the hydrogenation/etching process.

In the initial stage, gas-phase H-atoms impinge on both the carbon cap and the Ni_xC_y nanocluster (figure 1, *h*-cap). In the case of Ni_xC_y, the impinging H-atom diffuses on the cluster surface and either finds another H-adatom or connects to an incoming H-atom before H_2 desorption, according to the Langmuir–Hinshelwood (LH) recombinative desorption or the Eley–Rideal (ER) abstraction mechanisms, respectively [43-45]. Also, some H-adatoms can connect to the rim of the cap during their surface diffusion. We observe that incoming H-atoms preferable adsorb on the top of the cap, due to its relatively high curvature. This observation can be explained by the increase of the pyramidalization and misalignment of the π-orbitals of the C-atoms in this region [46]. In this stage, the hydrogen concentration rapidly increases, whereas the carbon concentration remains constant (figure 2a, C_{tot} and H). Consequently, mobile H-adatoms try to coalesce, leading to the occupation of neighbouring sites. While the electron interactions are not explicitly taken into account in our ReaxFF-based calculations, this observation corresponds well to DFT results, i.e., the association of H-adatoms is due to electron pairing and strain minimization, which is called the H-clustering effect [47]. This effect leads to a local amorphization of the cap carbon network where H-adatoms coalesce. The H-adatoms on the highly curved tip of the cap [46] and stressed rim of the cap [48] can subsequently change the ring distribution in the carbon cap. Indeed, we observe that the pentagon rings gradually disappear due to a pentagon (R5) – to – hexagon (R6) conversion (i.e., C-R5 to R6 with a barrier of 3.2 eV in DFT calculations [49]). Moreover, the number of both pentagons and hexagons can also fluctuate due to either incorporation of dissolved C-atoms into the cap or a dissolution of cap-edge C-atoms into the Ni-nanocluster (figure 2a and 2b). The drop of the number of pentagons eventually leads to a decrease of the cap curvature [50]. As a result, a network

consisting of nearly exclusively hexagons gradually covers the nanocluster surface, resulting in the formation of a carbon nanosheet at the end of the first stage.

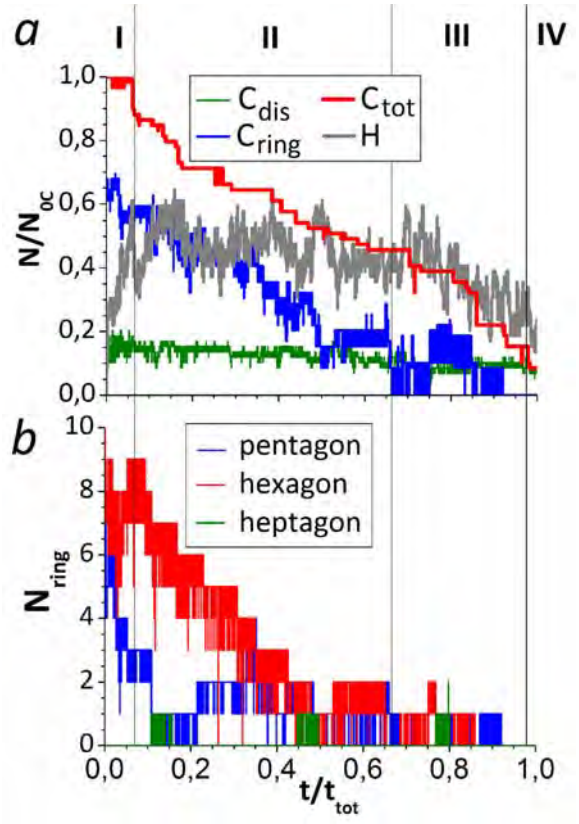

Figure 2 (*a*) Evolution of the averaged and normalized number of (dissolved C_{dis}, ring C_{ring} and total C_{tot}) carbon and hydrogen atoms during hydrogenation/etching of a (5,5) cap. The process is divided into four stages. (*b*) Evolution of the number of pentagons, hexagons and heptagons in the C cap network, as a function of the number of normalized MD&MC steps.

Stage II is characterized as the onset of the etching process. In this stage, the total number of carbon atoms drops continuously upon further hydrogenation (figure 2a, C_{tot}). Note, in contrast, that defective cap structures begin to lose their C-atoms already in stage I, and the first and

second stages are thus not distinguished for this case. In all cases, the number of hydrogen atoms rapidly increases in the first stage due to the high H-adsorption rate, before the number of adsorbed H-atoms saturates at the beginning of stage II (figure 2a, H). After the saturation (at which point it approximately equals half of the initial C number in the structures), their number is seen to fluctuate significantly, due to the etching and LH or/and ER desorption during the hydrogenation. In this stage, H-adatoms can weaken the Ni-C bonds at the cap-cluster interface and the high H-content eventually leads to breaking of some Ni-C bonds. The high H-concentration also allows to quickly terminate any dangling bonds of C-atoms at the nanostructure edge. As a result, the carbon nanosheet partially transforms to a carbon nanowall (or vertically-aligned graphene patches) (figure 1, stage II). In this conversion, the formation of 5-7 defects [51] can also be found [50] (figure 2b, stage II). However, such defects can also migrate or annihilate above 1500 K [52]. It is indeed experimentally known that hydrogen plays a major role in the formation of such free-standing graphene sheets, i.e., no carbon nanowalls are formed without H_2 gas flow or without irradiation by H radicals [53]. On the other hand, because of the competition between dehydrogenation, rehydrogenation and H-etching [29], either a nanowall or a nanosheet can be found one after the other on the catalyst surface [38, 54]. The formation of such unstable carbon structures was also detected during *in situ* transmission electron microscopy (TEM) observations before the appearance of a cap in SWNT growth from C_2H_2 precursors [27]. Also, in the case of larger nanoclusters, the nanosheet-nanowall conversion can be delayed, indicating a slightly stronger sheet-cluster interaction on the less-curved Ni surface area. While the horizontal graphene patches covering the surface are energetically favoured over their vertical free-standing counterparts in hydrocarbon-based CNT

growth [29], they are continuously destabilized due to the continuous in-flux of gas-phase H-atoms.

These structures eventually transform to simple carbon rings (i.e., hydrogen-containing pentagons or hexagons) [29, 38] and short carbon polyyne chains [29, 55, 56] at the beginning of stage III. Subsequently, only carbon chains remain (figure 2b, $t/t_{tot} > 0.9$) before the complete elimination of the carbon cap from the catalyst surface. This in turn allows incoming H-atoms to connect mostly with Ni atoms. Due to the relatively weak Ni-H interaction, H can move easily on the cluster surface and thus the H_2 desorption rate considerably increases in this stage. Consequently, the number of H-adatoms continuously drops in this stage (figure 2a, H, stage III).

In the fourth and final stage, the number of dissolved C-atoms starts to decreases as well due to their precipitation/segregation from the saturated nanocluster. Subsequently, all surface carbon atoms are eventually removed and only H-atoms are found on the now carbon-free nanocluster. While the system becomes less and less stable as the etching process progresses, i.e., the system energy increases from stage I to III, its value is nearly constant in the last stage of the H-assisted cap etching process. We found that the energy differences between the initial and final structures for the cases of ideal/defective caps on $Ni_{55}C_{19}$ and $Ni_{147}C_{46}$ nanoclusters are about 1.7 eV/atom and about 0.6 eV/atom, respectively. This indicates that the larger clusters are less destabilised than small clusters during the hydrogenation/etching of the caps.

The overall results indicate that the adsorption/desorption and etching nature is similar for different “cap + cluster” structures, including ideal caps of (5,5) with 40 C atoms and (10,0) tubes with 62 C atoms, as well as several defective caps on substrate-bounded $Ni_{55}C_{19}$ or $Ni_{147}C_{46}$ nanoclusters, although specific dissimilarities are found as well, as discussed above. In

general, we found that the etching nature of a carbon cap is similar to (the opposite of) the CNT nucleation process in hydrocarbon-based CNT growth [27, 29].

3.2 Destruction of carbon nanotubes. Our simulations indicate that the etching onset of SWNTs is different from the etching onset of a carbon cap as described above. In the initial step of the hydrogenation process of a SWNT, H atoms adsorb on the surface of the nanotube or catalyst cluster, similar to the case of a carbon cap. Due to the curvature effect, the adsorption barrier is lower than on graphene, and the nanotube reactivity is correspondingly higher [46]. Also, H adatoms simultaneously desorb as H_2 molecules from the system either by the LH or ER mechanism. Therefore, hydrogenation and dehydrogenation occur simultaneously before the CNT etching is initiated. Partial hydrogenation behaviour is also in agreement with experimental evidences, i.e., hydrogen is released by heating to 600°C-800°C [4, 8] and thus the nanotube surface is not fully covered by a "hydrogen shell" [57]. We find that the H-coverage on long nanotubes can reach up to maximum 30% before the etching initiates [32].

The clustering of hydrogen on the tube walls leads to sp^3 C atoms which have somewhat longer bond lengths than the sp^2 carbon atoms, thus leading to a local amorphization [24]. In agreement with DFT results, these amorphous sites are found in kink-steps of a chiral tube end-edge, as well as on the cap [48]. In contrast, in achiral (armchair and zigzag) SWNTs, the circumference of the tube end-edge is smoother than that of chiral tubes. Therefore, the cluster-tube interface is less reactive in the case of achiral tubes than their pentagon-containing cap region. Moreover, the tube end-edge is less stressed than the cap end-edges [48] and consequently H adatoms can be found on the entire tube surface, although their concentration is elevated in the cap region.

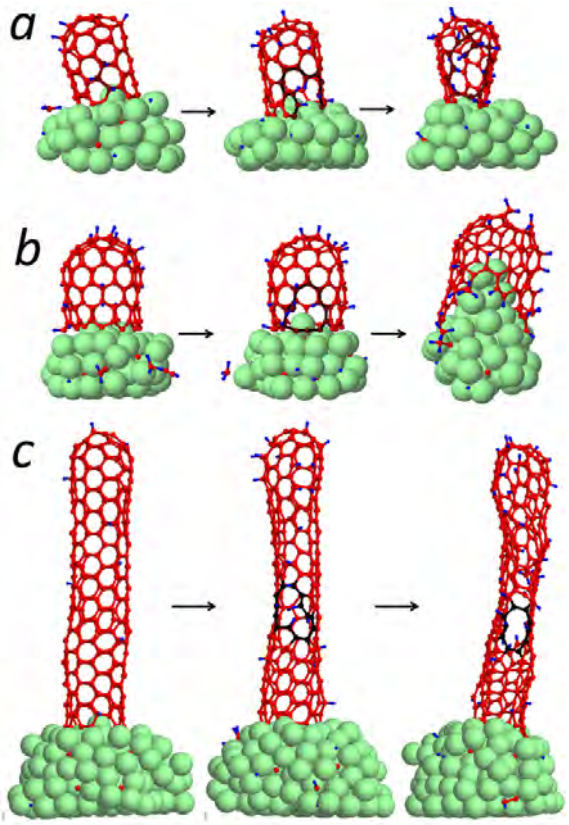

Figure 3 Short (*a*) armchair (5,5) and (*b*) zigzag (10,0) nanotubes as well as (*c*) long armchair (5,5) nanotube on a substrate-bound Ni cluster during H-impact. C atoms in the damaged regions are in black colours.

The etching onset is characterized by the eventual breaking of the more elongated HC-CH ortho bonds, which is also considered as the rate-limiting step of the hydrogenation/etching process [29]. Interestingly, the first C-C bond cleavage appears on the tube side-wall for both short and long CNTs, whereas their cap contains more H-adatoms (figure 3, second column). In our recent investigation, we found that the nature of the bond breaking event depends on the (γ) angle between the strained ortho HC-CH bond and the chirality vector of the ideal nanotube [32],

besides the curvature [23, 46] and metallicity effects [58-60]. This defect basically initiates the etching of both short and long CNTs, although it can also be healed again in the high-temperature hydrogenation of short CNTs in some cases. Consequently, the first C-C bonds are broken either in the cap side or near the tube end-edge in the case of a short CNT (figure 3a,b; last frames).

After the initial C-C breaking, new incoming gas-phase H-atoms can impinge on or diffuse to such defective or disordered sites. Subsequently, H-adatoms rapidly occupy nearby (neighbouring) C atoms in the bond breaking area, leading to the formation of a hole or so-called etch pit. The carbon-carbon bonds connecting these sites are then consecutively broken. This process closely resembles experimental evidence on graphite and MWNT etching, showing the formation of holes and etch pits upon H-atom exposure: the initial formation of an etch pit may occur at a site along the outer CNT wall that contains a defect [24].

Overall, three specific structures are consecutively distinguished in the hydrogenation/etching of a carbon tube: (i) a defect-free structure in the hydrogenation; (ii) a structure with initially broken C-C bonds and consecutive first etch pit or a hole; and finally (iii) damaged or H-etched tubes before their structure completely converts to carbon nanosheets, partially covering the catalyst surface. After the complete transformation of the carbon tube to a carbon nanosheet/nanowall, the remainder of the etching process resembles the etching of a carbon cap (figures 1-2, steps II-IV), as discussed in the previous section.

3.3 Distribution of etched species. During the hydrogenation and subsequent etching processes, the concentration of desorbed H_2 molecules is about three times higher than the concentration of gas-phase H-atoms (figure 4a).

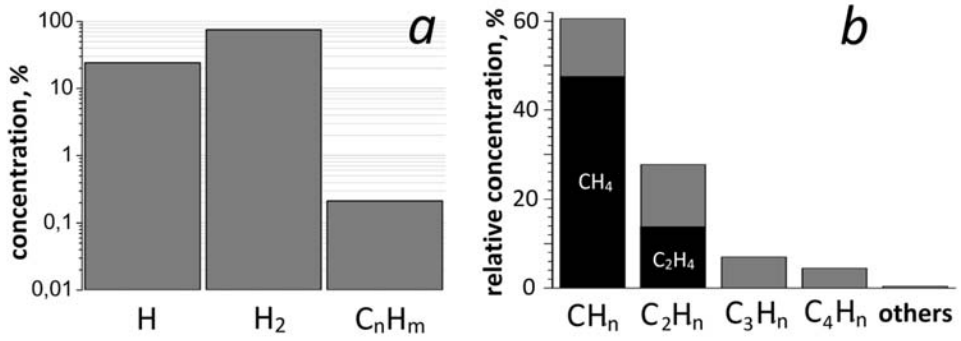

Figure 4 (*a*) Concentration of total desorbed/etched species and (*b*) relative concentration of the etched hydrocarbon C_nH_m species in the gas phase during the hydrogenation.

In addition to desorbed H_2 molecules, different types of etched hydrocarbon C_xH_y species can be found in the gas phase, albeit with very low concentrations (see Figure 4a) [26]. Amongst the etched hydrocarbon species, methane CH_4 and ethylene C_2H_4 molecules are the most abundant species (figure 4b) [61]. Also, the concentration of acetylene as well as CH_3 (due to the $CH_4+H\rightarrow CH_3+H_2$ reaction [62]) and acetylide C_2H radicals is significant during the etching process [26]. The overall results show that the distribution of etched species in the gas phase environment is in excellent qualitative agreement with experimental evidence of CNT growth from plasma CH_4/H_2 [20].

4. Conclusion

Using hybrid MD/MC simulations, we study the hydrogenation and subsequent etching of carbon nanotube caps, and small and long carbon nanotubes. The results indicate that the overall scenario of the cap etching by hydrogen plasma is similar to (the opposite of) SWNT nucleation from hydrocarbon C_nH_m species. During the hydrogenation/etching process, the carbon cap converts to a carbon nanosheet and subsequently to a carbon nanowall. Finally, carbon rings or short polyyne chains are sequentially found on the Ni cluster, before the elimination of the carbon cap. The overall analysis indicates that the adsorption/desorption and etching nature is very similar for different "cap/cluster" structures.

We found that the etching onset of SWNTs, however, is different from the etching onset of a carbon cap. During the hydrogenation, ortho H pairs play an important role in initiating the etching process on the tube side-wall, whereas mostly H-adatoms are found on the tube cap. After the initial damage formation, the nanotube eventually converts to a carbon nanowall or nanosheet and further etching steps can be explained by the etching stages of the carbon cap.

Also, we analysed the occurrence of various gas-phase C_xH_y species during the etching process. In the etching and dehydrogenation processes, CH_4 and C_2H_4 molecules are found as most abundant C_xH_y species in the gas phase, besides H-atoms and H_2 molecules. Overall, the entire hydrogenation / dehydrogenation / etching process is analysed in detail and compared with existing theoretical, simulation and experimental data.

In general, this study leads to a better understanding of the individual effect of H-radicals on the CNT etching in a plasma environment and it provides a nanoscale analysis of the etching nature of catalysed base-grown CNTs.

Acknowledgments

U. K. gratefully acknowledges financial support from the Fund of Scientific Research Flanders (FWO), Belgium (Grant No. 12M1315N). The work was carried out in part using the Turing HPC infrastructure of the CalcUA core facility of the Universiteit Antwerpen, a division of the Flemish Supercomputer Centre VSC, funded by the Hercules Foundation, the Flemish Government (department EWI) and the Universiteit Antwerpen. The authors also thank Prof. A. C. T. van Duin for sharing the ReaxFF code.

References

1. Tessonnier J-P, Su DS. Recent Progress on the Growth Mechanism of Carbon Nanotubes: A Review. ChemSuSChem 2011; 4: 824.
2. Neyts EC. PECVD growth of carbon nanotubes: From experiment to simulation. J Vac Sci Technol B 2012; 30: 030803.
3. Jourdain V, Bichara C. Current understanding of the growth of carbon nanotubes in catalytic chemical vapour deposition. Carbon 2013; 58: 2.
4. Page AJ, Ding F, Irle S, Morokuma K. Insights into carbon nanotube and graphene formation mechanisms from molecular simulations: a review. Rep Prog Phys 2015; 78: 036501.
5. Moisala A, Nasibulin AG, Kauppinen EI. The role of metal nanoparticles in the catalytic production of single-walled carbon nanotubes - a review. J Phys Condens Matter 2003; 15: S3011.

6. MacKenzie KJ, Dunens OM, Harris AT. An Updated Review of Synthesis Parameters and Growth Mechanisms for Carbon Nanotubes in Fluidized Beds. Ind Eng Chem Res 2010; 49: 5323.
7. Kong J, Cassell AM, and Dai H. Chemical vapor deposition of methane for single-walled carbon nanotubes. Chem Phys Lett 1998; 292: 567.
8. Maruyama S, Kojima R, Miyauchi Y, Chiashi S, and Kohno M. Low-temperature synthesis of high-purity single-walled carbon nanotubes from alcohol. Chem Phys Lett 2002; 360: 229.
9. Dai H., Rinzler AG, Nikolaev P, Thess A, Colbert DT, and Smalley RE, Single-wall nanotubes produced by metalcatalyzed disproportionation of carbon monoxide. Chem Phys Lett 1996; 260: 471.
10. Tibbetts GG. Growing carbon fibers with a linearly increasing temperature sweep: experiments and modelling. Carbon 1992; 30: 399.
11. Ren ZF, Huang ZP, Xu JW, Wang JH, Bush P, Provencio PN. Synthesis of large arrays of well-aligned carbon nanotubes on glass. Science 1998; 282: 1105.
12. Chhowalla M, Teo KBK, Ducati C, Rupesinghe NL, Amaratunga GAJ, Ferrari AC, Roy D, Robertson J, and Milne WI. Growth process conditions of vertically aligned carbon nanotubes using plasma enhanced chemical vapor deposition. J Appl Phys 2001; 90: 5308.
13. Delzeit L, Nguyen CV, Stevens RM, Han J, and Meyyappan M. Growth of carbon nanotubes by thermal and plasma chemical vapour deposition processes and applications in microscopy. Nanotechnology 2002; 13: 280.

14. Hirata T, Satake N, Jeong C-H, Kato T, and Hatakeyama R. Magnetron type radio-frequency plasma control yielding vertically well aligned carbon nanotube growth. Appl Phys Lett 2003; 83: 1119.
15. Bower C, Zhu W, Jin S, and Zhou O. Plasma-induced alignment of carbon nanotubes. Appl Phys Lett 2000; 77: 830.
16. Merkulov VI, Melechko AV, Guillorn MA, Lowndes DH, and Simpson ML. Alignment mechanism of carbon nanofibers produced by plasma-enhanced chemical vapor deposition. Appl Phys Lett 2001; 79: 2970.
17. Hofmann S, Ducati C, Robertson J, and Kleinsorge B. Low temperature growth of carbon nanotubes by plasma-enhanced chemical vapor deposition. Appl Phys Lett 2003; 83: 135.
18. Min YS, Bae EJ, Oh BS, Kang D, and Park W. Low-temperature growth of single-walled carbon nanotubes by water plasma chemical vapor deposition. J Amer Chem Soc 2005; 127: 12498.
19. Hofmann S, Ducati C, Kleinsorge B, and Robertson J. Direct growth of aligned carbon nanotube field emitter arrays onto plastic substrates. Appl Phys Lett 2003; 83: 4661.
20. Hash DB and Meyyappan M. Model based comparison of thermal and plasma chemical vapor deposition of carbon nanotubes. J Appl Phys 2003; 93: 750.
21. Kato T and Hatakeyama R. Growth of Single-Walled Carbon Nanotubes by Plasma CVD. Journal of Nanotechnology 2010; 2010: 1.
22. Zhang G, Mann D, Zhang L, Javey A, Li Y, Yenilmez E, Wang Q, et al. Ultra-high-yield growth of vertical single-walled carbon nanotubes: Hidden roles of hydrogen and oxygen. PNAS 2005; 102: 16141.

23. Zhang G, Qi P, Wang X, Lu Y, Li X, Tu R. et al. Selective Etching of Metallic Carbon Nanotubes by Gas-Phase Reaction. Science 2006; 304: 974.
24. Behr MJ, Gaulding EA, Mkhoyan KA, Aydil ES, Hydrogen etching and cutting of multiwall carbon nanotubes. J Vac Sci Technol B 2010; 28: 1187.
25. Hou P-X, Li W-S, Zhao S-Y, Li G-X, Shi C, Liu C, Cheng H-M. Preparation of Metallic Single-Wall Carbon Nanotubes by Selective Etching. ACS Nano 2014; 8: 7156.
26. Okita A, Suda Y, Oda A, Nakamura J, Ozeki A, Bhattacharyya K. et al. Effects of hydrogen on carbon nanotube formation in CH_4/H_2 plasmas. Carbon 2007; 45: 1518.
27. Yoshida H, Takeda S, Uchiyama T, Kohno H and Homma Y. Atomic-Scale In-situ Observation of Carbon Nanotube Growth from Solid State Iron Carbide Nanoparticles. Nano Lett 2008; 8: 2082.
28. Hofmann S, Sharma R, Ducati C, Du G, Mattevi C, Cepek C. et al. In situ Observations of Catalyst Dynamics during Surface-Bound Carbon Nanotube Nucleation. Nano Lett 2007; 7: 602.
29. Khalilov U, Bogaerts A and Neyts EC. Atomic scale simulation of carbon nanotube nucleation from hydrocarbon precursors. Nat Commun 2015; 6: 10306.
30. Rao F-B, Li T & Wang Y-L. Effect of hydrogen on the growth of single-walled carbon nanotubes by thermal chemical vapor deposition. Phys E 2008; 40: 779.
31. Harutyunyan AR, Chen G, Paronyan TM, Pigos EM, Kuznetsov OA, Hewaparakrama K. et al. Preferential growth of single-walled carbon nanotubes with metallic conductivity. Science 2009; 326: 116.

32. Khalilov U, Bogaerts A, Xu B, Kato T, Kaneko T and Neyts EC. How the alignment of adsorbed ortho H pairs determines the onset of selective carbon nanotube etching. Nanoscale 2017; 9: 1653.
33. Mees MJ, Pourtois G, Neyts EC, Thijsse BJ, Stesmans A. Uniform-acceptance force-bias Monte Carlo method with time scale to study solid-state diffusion. Phys Rev B 2012; 85: 134301.
34. Bal KM, Neyts EC. On the time scale associated with Monte Carlo simulations. J Chem Phys 2014; 141: 204104.
35. Bussi G, Donadio D, Parrinello M. Canonical sampling through velocity-rescaling. J Chem Phys 2007; 126: 014101.
36. Mueller JE, van Duin ACT, Goddard III WA. Development and Validation of ReaxFF Reactive Force Field for Hydrocarbon Chemistry Catalyzed by Nickel. J Phys Chem C 2010; 114: 4939.
37. Neyts EC, Shibuta Y, van Duin ACT, Bogaerts A. Catalyzed Growth of Carbon Nanotube with Definable Chirality by Hybrid Molecular Dynamics Force Biased Monte Carlo Simulations. ASC Nano 2010; 4: 6665.
38. Khalilov U, Bogaerts A, Neyts EC. Microscopic mechanisms of vertical graphene and carbon nanotube cap nucleation from hydrocarbon growth precursors. Nanoscale 2014; 6: 9206.
39. Fiawoo M-F C, Bonnot A-M, Amara H, Bichara C, Thibault-Penisson J, and Loiseau A. Evidence of Correlation between Catalyst Particles and the Single-Wall Carbon Nanotube Diameter: A First Step towards Chirality Control. Phys Rev Lett 2012; 108: 195503.

40. Zhu WM, Borjesson A, Bolton K. DFT and tight binding Monte Carlo calculations related to single-walled carbon nanotube nucleation and growth. Carbon 2010; 48: 470.
41. Nasibulin AG, Pikhitsa PV, Jiang H, Kauppinen EI. Correlation between catalyst particle and single-walled carbon nanotube diameters. Carbon 2005; 43: 2251.
42. Despiau-Pujo E, Davydova A, Cunge G, Graves DB. Hydrogen Plasmas Processing of Graphene Surfaces. Plasma Chem Plasma Process 2016; 36: 213.
43. Sha X, Jackson B, Lemoine D. Quantum studies of Eley-Rideal reactions between H atoms on a graphite surface. J Chem Phys 2002; 116: 7158.
44. Zecho T, Güttler A, Sha X, Lemoine D, Jackson B, Küppers J. Abstraction of D chemisorbed on graphite (0001) with gaseous H atoms. Chem Phys Lett 2002; 366: 188.
45. Neyts EC. Plasma-Surface Interactions in Plasma Catalysis. Plasma Chem Plasma Process 2016; 36: 185.
46. Niyogi S, Hamon MA, Hu H, Zhao B, Bhowmik P, Sen R, Itkis ME, Haddon RC. Chemistry of Single-Walled carbon Nanotubes. Acc Chem Res 2002; 35: 1105.
47. Andreoni W, Curioni A, Kroes JMH, Pietrucci F, Gronin O. Exohedral Hydrogen Chemisorption on a Carbon Nanotube: The Clustering Effect. J Phys Chem C 2012; 116: 269.
48. Wang Q, Wang H, Wei L, Yang S-W and Chen Y. Reactive Sites for Chiral Selective Growth of Single-Walled Carbon Nanotubes: A DFT Study of Ni_{55}−C_n Complexes, J Phys Chem A 2012; 116: 11709.
49. Dumlich H, A Path to Monochiral Ensembles of Carbon Nanotubes and their Properties, PhD Thesis, Berlin, Germany, 2013.

50. Iijima S, Ajayan PM, Ichihashi T. Growth Model for Carbon Nanotubes, Phys Rev Lett 1992; 69: 3100.
51. Collins PG. Defects and disorder in carbon nanotubes, in Oxford Handbook of Nanoscience and Technology: Frontiers and Advances. Narlikar AV & Fu YY, Eds. (Oxford Univ. Press, Oxford, 2009).
52. Krasheninnikov AV, Nordlund K, and Keinonen J. Production of defects in supported carbon nanotubes under ion irradiation. Phys Rev B 2002; 65: 165423.
53. Kondo H, Hori M and Hiramatsu M (2011). Nucleation and Vertical Growth of Nano Graphene Sheets, Graphene - Synthesis, Characterization, Properties and Applications, Prof. Jian Gong (Ed.), ISBN: 978-953-307-292-0, InTech, Available from: http://www.intechopen.com/books/graphene-synthesischaracterization-properties-and-applications/nucleation-and-vertical-growth-of-nano-graphene-sheets
54. Wang Y, Gao X, Qian H-J, Ohta Y, Wu X, Eres G, Morokuma K, Irle S. Quantum chemical simulations reveal acetylene-based growth mechanisms in the chemical vapor deposition synthesis of carbon nanotubes. Carbon 2014; 72: 22.
55. Eres G, Rouleau CM, Yoon M, Puretzky AA, Jackson JJ, and Geohegan DB. Model for self-assembly of carbon nanotubes from acetylene based on real-time studies of vertically aligned growth kinetics. J Phys Chem C 2009; 113: 15484.
56. Arifin R, Shibuta Y, Shimamura K, Shimojo F & Yamaguchi S. Ab initio molecular dynamics simulation of ethylene reaction on nickel (111) surface. J. Phys Chem C 2015; 119: 3210.
57. Liu C, Fan YY, Liu M, Cong HT, Cheng HM, Dresselhaus MS. Hydrogen Storage in Single-Walled Carbon Nanotubes at Room Temperature. Science 1999; 286: 1127.

58. Hamada N, Sawada S, Oshiyama A. New one-dimensional conductors-graphitic microtubules. Phys Rev Lett 1992; 68: 1579.
59. Saito R, Fujita M, Dresselhaus G, Dresselhaus MS. Electronic structure of chiral graphene tubules. Appl Phys Lett 1992; 60: 2204.
60. Joselevich E, Electronic Structure and Chemical Reactivity of Carbon Nanotubes: A Chemist's View. Chem Phys Chem 2004; 5: 619.
61. Liu Q, Ren W, Chen Z-G, Wang D-W, Liu B. et al., Diameter-Selective Growth of Single-Walled Carbon Nanotubes with High Quality by Floating Catalyst Method. ACS Nano 2008; 2: 1722.
62. Meyyappan M, Delzeit L, Cassell A, Hash D. Carbon Nanotube Growth by PECVD: A Review. Plasma Sources Sci Technol 2003; 12: 205.